Partial Differential Equations in Applied Mathematics 11 (2024) 100798

Contents lists available at ScienceDirect

Partial Differential Equations in Applied Mathematics

journal homepage: www.elsevier.com/locate/padiff

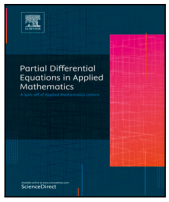

Analytical and numerical study of diffusion propelled surface growth phenomena

E. Kovács [a,*], I.F. Barna [b], G. Bognár [a], L. Mátyás [c], K. Hriczó [a]

[a] University of Miskolc, Miskolc-Egyetemváros, 3515, Hungary
[b] Hungarian Research Network Wigner Research Centre for Physics, Konkoly-Thege Miklós út 29 - 33, 1121 Budapest, Hungary
[c] Department of Bioengineering, Faculty of Economics, Socio-Human Sciences and Engineering, Sapientia Hungarian University of Transylvania, Libertății sq. 1, 530104 Miercurea Ciuc, Romania

ARTICLE INFO

Keywords:
Kardar–Parisi–Zhang equation
Growth models
Noise term
Diffusion
Self-similar method
Explicit time-integration

ABSTRACT

To understand the complex problem of surface growth phenomena, we developed a model in which the regular diffusion equation is coupled to the Kardar–Parisi–Zhang (KPZ) equation. The fundamental or Gaussian solution of the regular diffusion equation is considered as an external noise or source term in the KPZ equation. The obtained system of partial differential equations is analytically solved by a self-similar Ansatz and expressed the solution as a combination of elementary and special functions. Using this solution, the effects of the physical parameters were explicitly investigated. Our recent explicit numerical method, the leapfrog-hopscotch algorithm, is also tested for this problem. It is shown that this method can be safely used with orders of magnitude larger time step sizes than the usual explicit (Euler) scheme as well if we are far from the cusp-like solutions. We pointed out that the cusps themselves cannot be properly simulated by any method that we know.

1. Introduction

The phenomena of surface growth are fascinating and complex problems from both a scientific and engineering point of view. The literature on the subject is vast, so we will mention only a few important summary works (see[1–3]). Several mathematical models can describe the growing process. However, if we try to describe and understand the phenomenon, which is part of a more complex process and takes place in parallel with other dynamic processes, we do not find much information in the scientific literature. A typical example is hydrodynamics, where at least mass and momentum transport are usually coupled; see, for example, Euler's equations. Coupling and studying surface growth as an integral part of a complete hydrodynamic model is a challenging topic. In the following, we present a more modest (but fully analytical) path, where we couple regular diffusion (as the source of noise) with the well-known KPZ[4] surface growth equation. For a simple and transparent description, we use Cartesian coordinates and one spatial dimension. In our next model we apply the self-similar Ansatz,[5] which is a powerful tool, to reduce the original coupled non-linear partial differential equation (PDE) system to an ordinary differential equation (ODE) system, which can be successfully solved with analytic means. In the last decades we investigated numerous dynamical systems, like viscous fluids,[6] non-linear electrodynamics[7] or quantum mechanics[8] with the self-similar Ansatz and presented physically relevant finite and disperse solutions. One may also find applications when the Cattaneo–Christov theory is used in the topic of viscous fluids[9] or nanofluids.[10,11] We have to mention two studies which are the direct forerunners of the present work. In the first one, we investigated the KPZ equation with four different kinds of colour, Gaussian and Lorenzian noise terms and we presented fully analytic results with in-depth parameter dependence analysis.[12] We must highlight that the case of the Gaussian noise has an analytic solution. Based on these analytic results detailed numerical investigations were also performed by our group.[13–15]

The second precursor is a recent publication,[16] in which we have filled a gap and presented additional solutions to the regular diffusion equation using the self-similar Ansatz, in addition to the basic Gaussian solutions. Such non-trivial but simple solutions for non-regular diffusion had not been presented before that work. Meanwhile, new numerical algorithms were developed in[17–19] for solving the diffusion or heat-conduction equation. These are explicit schemes which are unconditionally stable for the linear diffusion equation. These algorithms were extensively tested for numerous irregular diffusion equations where the diffusion coefficient had various temporal and spatial dependencies, and the stiffness of the problem is very high.[20–22] It turned out that in most cases, the leapfrog-hopscotch (LH) method is

* Corresponding author.
E-mail address: endre.kovacs@uni-miskolc.hu (E. Kovács).

https://doi.org/10.1016/j.padiff.2024.100798
Received 14 March 2024; Received in revised form 20 May 2024; Accepted 1 July 2024
Available online 4 July 2024

the most effective. Most of the algorithms have already been generalized to potentially more complicated equations related to diffusion, for example, the nonlinear Fisher's Equation[23] and we have the hope that other nonlinear equations can also be solved with them.

The first goal of our recent study is to provide in-depth analytical and numerical analysis for a KPZ equation, where the driving term is the Gaussian solution of the regular diffusion equation. We will show that the analytic solutions can have cusps where the solutions become infinite. This experience is consistent with the rigorous proof of Muravnik who proved the absence of global positive solutions of the KPZ equation.[24] The second main goal of this work is to explore the applicability of the most efficient LH algorithm to this nonlinear problem. We will demonstrate that although the LH method is very efficient in large parameter regions, it is unable to provide the solution within the specified error close to the cusps. However, the solutions remain finite, and the corresponding temporal and spatial derivatives have finite values too. This is our first investigated model, where this numerical method fails in a few specific parameter regions. We have to mention that numerous similar systems like fractional diffusion, fractional porous media or fractional reaction–diffusion equations were investigated with various numerical methods like.[25–28]

2. The applied model

In the model under study, the regular diffusion and KPZ equation are used. The KPZ equation indicates the mechanism of surface growth, and it has on the r.h.s a Laplace term related to the spreading and diffusion, a nonlinear term related to the first derivative of the surface level and an additional term related to an external source. The concentration derived from the first equation is used as additive noise or, in other words, as a source condition in the second, KPZ equation:

$$\frac{\partial C(x,t)}{\partial t} = D\frac{\partial^2 C(x,t)}{\partial t^2}, \tag{1}$$

$$\frac{\partial h(x,t)}{\partial t} = \nu\frac{\partial^2 h(x,t)}{\partial x^2} + \frac{\lambda}{2}\left(\frac{\partial h(x,t)}{\partial x}\right)^2 + t^{-\frac{1}{2}}\cdot C(x,t), \tag{2}$$

where C denotes the concentration, h is the height function, D is the diffusion coefficient and the parameter ν determines the surface tension, while λ is proportional to the average growth velocity. The first term on the right hand side of Eq. (2) describes relaxation of the interface by a surface tension, which prefers a smooth surface. The second term is the lowest-order nonlinear term that can appear in the surface growth equation justified with the Eden model and originates from the tendency of the surface to locally grow normal to itself and has a non-equilibrium in origin. The third term is a Langevin noise one which mimic the stochastic nature of any growth process and has usually a Gaussian distribution. To obtain an unequivocal dispersive self-similar solution, an additional $t^{-1/2}$ time-dependent factor has been included in the KPZ equation, which makes the model explicitly time-dependent or in other words, non-autonomous. This is an interesting feature of our model. In our previous scientific work, we have already encountered a non-autonomous PDE,[16] derived from a time-dependent generalization of the Cattaneo–Vernotte equation (non-Fourier heat conduction). That led to the Euler–Poisson–Darboux PDE, which takes the form of a telegraph wave equation with an extra $1/t$ time dependence at the first time-derivative term. To the best of our knowledge, there is no general theory for non-autonomous PDEs. However, for non-autonomous ODEs some monographs are available.[29–31]

To derive analytically, disperse, physically relevant solutions to (1), we apply two self-similar Ansätze[5] of the form:

$$C(x,t) = t^{-\alpha}g\left(\frac{x}{t^\beta}\right) = t^{-\alpha}g(\omega), \qquad h(x,t) = t^{-\gamma}f\left(\frac{x}{t^\beta}\right) = t^{-\gamma}f(\omega). \tag{3}$$

All the similarity exponents α, β and γ are of primary physical importance since $\alpha and \gamma$ represent the rate of decay of the magnitude of the corresponding variable, while β is the rate of spread (or contraction if $\beta < 0$) of the space distribution for $t > 0$. The most powerful result of this Ansatz is the fundamental or Gaussian solution of the Fourier heat conduction equation (or for Fick's diffusion equation) with $\alpha = \beta = 1/2$. This transformation is based on the assumption that a self-similar solution exists, i.e., every physical parameter preserves its shape during the expansion. Self-similar solutions usually describe the asymptotic behaviour of an unbounded or a far-field problem; the time t and the space coordinate x appear only in the combination of $f(x/t^\beta)$. It means that the existence of self-similar variables implies the lack of characteristic length and time scales.

The properties of these two trial functions were discussed in our former studies[6,12,16] also. The functions $f(\omega)$ and $g(\omega)$ are called shape functions and must have appropriate smoothness. The corresponding derivatives of function $C(x,t)$ are as follows

$$\frac{\partial C}{\partial t} = -\alpha t^{-\alpha-1}g(\omega) - \beta t^{-\alpha-1}\omega\frac{\partial g}{\partial \omega} \tag{4}$$

$$\frac{\partial^2 C}{\partial x^2} = t^{-\alpha-2\beta}\frac{\partial^2 g}{\partial \omega^2} \tag{5}$$

Applying Ansatz (3) to the PDE system of (1)–(2) as it is presented in the equations above, the next coupled ODE system can be derived

$$-\frac{1}{2}g - \frac{1}{2}\omega g' = Dg'', \tag{6}$$

$$\nu f''(\omega) + f'(\omega)\left[\frac{\omega}{2} + \frac{\lambda}{2}f'(\omega)\right] + g = 0. \tag{7}$$

For the self-similar exponents, the following relations have to be fulfilled

$$\alpha = \frac{1}{2}, \beta = \frac{1}{2}, \gamma = 0. \tag{8}$$

According to these conditions, we have

$$\omega = \frac{x}{\sqrt{t}}. \tag{9}$$

By choosing the proper initial conditions for the first diffusion equation we can get the usual Gaussian solution

$$g = ae^{\frac{-\omega^2}{4D}}, \tag{10}$$

where a is a constant. At this point, we have to emphasize that for an arbitrary real α and for $\beta = 1/2$, the solutions become much more complicated and can be expressed with Kummer's functions. The properties of the solutions are exhaustively analysed in our latest study.[16] With this knowledge, the final form of the ODE obtained with the shape function of the KPZ equation can be given as follows

$$\nu f''(\omega) + \frac{f'(\omega)}{2}\left[\omega + \lambda f'(\omega)\right] + ae^{\frac{-\omega^2}{4D}} = 0. \tag{11}$$

After an exhaustive investigation, we may state that there is no general formula available when all the four parameters λ, η, a and D have arbitrary numerical values. Fortunately, if the constrain $4D = 2\nu$ holds the ODE has a simplified form of

$$\nu f''(\omega) + \frac{f'(\omega)}{2}\left[\omega + \lambda f'(\omega)\right] + ae^{\frac{-\omega^2}{2\nu}} = 0. \tag{12}$$

We tried numerous parameter sets, but only this relation gives analytic results. If any other numerical values are given for D then there is no analytic solution available, so numerical methods have to be applied.

3. Results

In the next subsections, we present the results of our analytic and numerical analysis of Eq. (12). First, we give an analytic expression followed by a detailed parameter study and a stability analysis of the parameters. Later, we apply the leapfrog-hopscotch (LH) and the explicit (Euler) or, in other words, the forward-time central-space (FTCS) scheme to solve the PDE system (1)–(2).

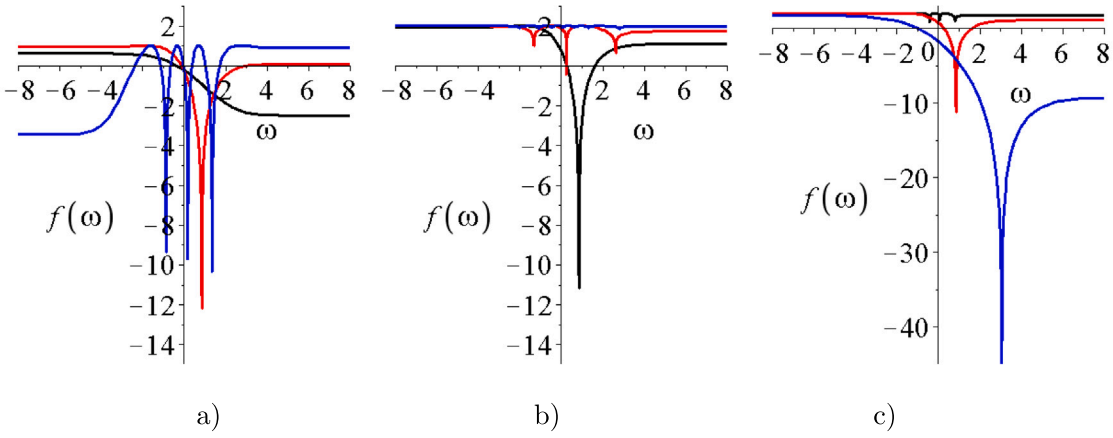

Fig. 1. The shape functions $f(\omega)$ of Eq. (13) for various $\{a, \lambda, \nu\}$ parameter sets. In Fig. 1. (a), the black, red and blue lines are for the $\{0.1, 1, 1\}, \{1, 1, 1\}, \{20, 1, 1\}$ numerical parameter sets, in Fig. 1. (b). the parameter sets are changed to $\{1, 1, 1\}, \{1, 10, 1\}, \{1, 70, 1\}$ numerical sets, and in Fig. 1. (c), the parameter sets are changed to $\{1, 1, 0.1\}, \{1, 1, 1\}, \{1, 1, 3\}$, respectively. The integration constants $C_1 = 1$ and $C_2 = 2$ are the same for all three curves. (For interpretation of the references to colour in this figure legend, the reader is referred to the web version of this article.)

3.1. Analytical solutions

Using the Maple 12 mathematical software package, the next closed expression for the solution can be derived

$$f(\omega) = -\frac{\nu}{\lambda} \ln\left(1 + \left[\tan\left\{\frac{\sqrt{2\lambda a\pi}\cdot erf(\frac{\omega}{2\sqrt{\nu}}) + 2C_1\sqrt{\nu}}{2\sqrt{\nu}}\right\}\right]^2\right) + C_2, \tag{13}$$

where erf denotes the error function. To learn more mathematical properties of this function, consult the handbook of.[32] Note, that the expression depends on all three strength parameters λ, ν, a, and C_1, C_2 are the free integration constants. Fig. 1 presents various solutions for different values of $\{a, \lambda, \nu\}$. The properties of these curves are far from being trivial. It seems to be clear that the larger the strength of the Gaussian source term a the larger the number of the cusps. The role of the second two parameters are however not so clear to see. We can understand these properties on Fig. 2 later, if the $\nu - \lambda$ parameter pairs are closer to a singularity than the cusp becomes deeper and deeper. It is important to emphasize that due to the properties of the tan function, the solutions may go to infinity with infinite first derivatives at given points. The presented plots show, however, only finite singularities; this is due to the Maple 12 software.

To have a deeper understanding of the solutions, Eq. (13) has to be investigated in detail. The tangent function becomes singular if the argument is equal to $(2n-1)\pi/2$ where n is an integer. Consider first the case that $C_1 = 0$. The error function is bounded between 0 and +1. Analysing the argument of the *tan* function, it can be easily evaluated that singularities occur for large ω if the relation of $\sqrt{\lambda a\pi/(2\nu)} = (2n-1)\pi/2$ is fulfilled.

Fixing the values of $2a\pi = 1$ and $\omega = 1$, which provide the strength of the noise term and an arbitrary position of the shape function, the number of free parameters is reduced to two. In such cases, a stability analysis can be performed for the function

$$\tan\left[\frac{\sqrt{\lambda}erf(1/2\nu)}{2\sqrt{\nu}}\right]. \tag{14}$$

The stability chart of (14) is visualized on Fig. 2 for λ and μ intervals. The rainbow regions show where the function has well-defined finite values, and the black solid lines show the singularities. White regions represent large finite values. The periodicity of the above-discussed singularities is clearly visible. This type of stability analysis is quite common, *e.g.* for Mathieu functions,[33] and needs to be classified as periodic or divergent for certain parameter pairs.

Now consider the case when $C_1 \neq 0$ together that $\sqrt{\lambda a\pi(2\nu)} < \frac{\pi}{2}$. If we examine the argument of the tangent function more closely, we can see that the upper value of the error function is one. If the constant C_1 after the error function is small enough, it means that the result is still continuous, and it is finite for any finite $\zeta = \omega/(2\sqrt{\nu})$, which is presented in Fig. 3.

In case when C_1 becomes larger, the argument of the tangent may pass $\pi/2$ and at this point, divergences appear in its value.

These phenomena are similar to phase transitions in which a transition occurs in the behaviour of the system at certain values of the order parameter. This effect can be clearly seen in Fig. 4.

Our analysis clearly shows that the solutions have a very rich mathematical structure and are far from trivial.

Fig. 5 presents the solution of the KPZ equation, the height $h(x,t)$ of the growing surface for the three parameter sets. On the right-hand side figure, the distinct islands are clearly visible, whereas the valleys between each island are, in fact, infinitely deep.

3.2. Numerical solutions

In this subsection we present our results obtained with numerical means. We performed different calculations with the LH Algorithms and with the FTCS scheme. First, we specify the time- and space-discretization and then the used numerical algorithms.

Description of the numerical procedures applied

The time axis is uniformly discretized, which means $t \in [t^0\ ,\ t^{fin}]$, and

$$t^n = t^0 + n\Delta t,\ \ n = 1, \dots, T,\ \ \ T\Delta t = t^{fin} - t^0. \tag{15}$$

An equidistant spatial mesh is used on the interval $x \in [x_0\ ,\ x_N = x_0 + L] \subset \mathbb{R}$ as follows

$$x_j = x_0 + j\Delta x,\ j = 0, \dots, N,\ N\Delta x = L. \tag{16}$$

The considered space and time domain will be specified when the numerical case studies are presented. After the application of the most frequent central difference formulas for the first and second space derivatives in Eqs. (1) and (2), we obtain two ODE systems for the node variables:

$$\frac{dC_i}{dt} = D\frac{C_{i-1} - 2C_i + C_{i+1}}{\Delta x^2}, \tag{17}$$

and

$$\frac{dh_i}{dt} = \nu\frac{h_{i-1} - 2h_i + h_{i+1}}{\Delta x^2} + \frac{\lambda}{8}\left(\frac{h_{i+1} - h_{i-1}}{\Delta x}\right)^2 + C_i/\sqrt{t}. \tag{18}$$

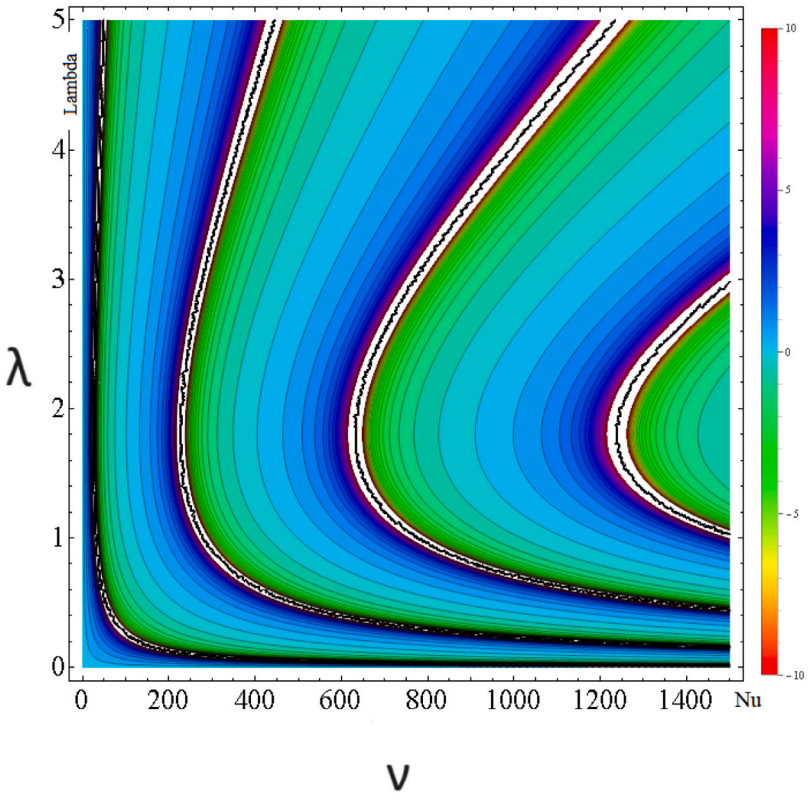

Fig. 2. The stability of the function of Eq. (14) in the parameter ranges of $0 \le \nu \le 150$ and $0 \le \lambda \le 5$, respectively. In the white regions, the investigated function lies outside the range of [−10..10], while at the solid black lines, the function has singular values.

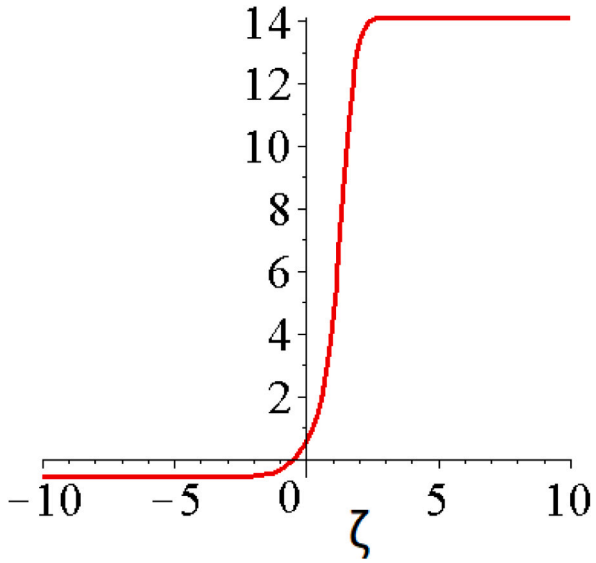

Fig. 3. The function $tan(erf(\zeta) + C_1)$, where $C_1 = 0.5$. One can see, that the functions is still finite and continuous.

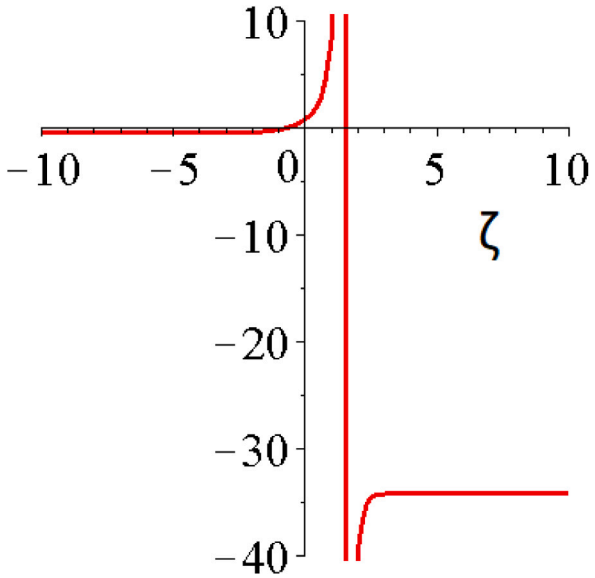

Fig. 4. The function $tan(erf(\zeta) + C_1)$ for $C_1 = 0.6$. At this form the tangent function yields a divergence.

In the case of the Explicit Euler time discretization, the forward difference formula is applied to the left side, while the whole right side is taken at the old time level. This yields the FTCS schemes for Eq. (1):

$$C_i^{n+1} = C_i^n + r_i(C_{i-1}^n - 2C_i^n + C_{i+1}^n), \tag{19}$$

and, for Eq. (2):

$$h_i^{n+1} = h_i^n + 2r_2(h_{i-1}^n - 2h_i^n + h_{i+1}^n) + r_3(h_{i+1}^n - h_{i-1}^n)^2 + C_i\Delta t/\sqrt{t^n}, \tag{20}$$

where $r_i = D\frac{\Delta t}{\Delta x^2}$, $r_2 = \nu\frac{\Delta t}{\Delta x^2}$, and $r_3 = \frac{\lambda}{8}\frac{\Delta t}{\Delta x^2}$ can be called mesh ratios for the different interactions.

When applying the leapfrog-hopscotch method, the odd and even nodes must be treated differently. We start with a half-sized time step for only the nodes with odd space index using the initial C_i^0 and h_i^0

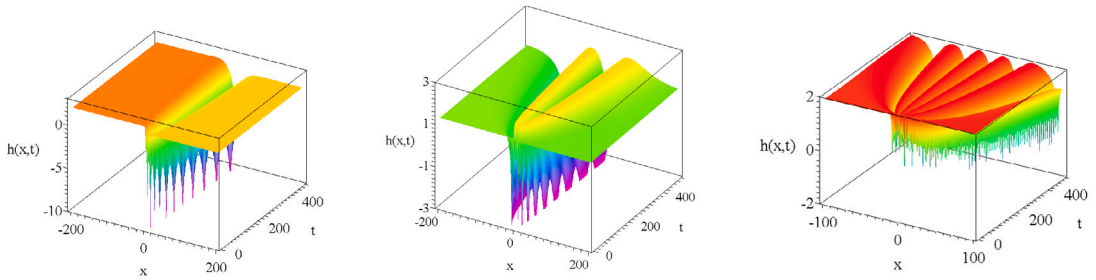

Fig. 5. The solutions $h(x,t)$ to Eq. (2) for three specific parameter sets. From left to right (a) $\{1,1,1\}$, (b) $\{4,8,5\}$, (c) $\{8,20,4\}$ and the integration constants are fixed for all three cases $C_1 = 1$, $C_2 = 2$.

values, which are substituted to the formulas

$$C_i^{1/2} = \frac{C_i^0 + \frac{r_1}{2}\left(C_{i-1}^0 + C_{i+1}^0\right)}{1 + r_1}, \tag{21}$$

and for Eq. (2):

$$h_i^{1/2} = \frac{h_i^0 + r_2\left(h_{i-1}^0 + h_{i+1}^0\right)/2 + r_3\left(h_{i+1}^0 - h_{i-1}^0\right)^2 + C_i^{1/2}\Delta t/\left(2\sqrt{t}\right)}{1 + r_2}. \tag{22}$$

After this, the Dirichlet boundary conditions are upgraded (nodes 0 and N, thus N should be even). Now the internal even nodes come: full time steps must be made for them with the formulas

$$C_i^{n+1} = \frac{(1 - r_1)C_i^n + r_1(C_{i-1}^{n+1/2} + C_{i+1}^{n+1/2})}{1 + r_1}, \tag{23}$$

and, for Eq. (2)

$$h_i^{n+1} = \frac{(1 - r_2)h_i^n + r_2(h_{i-1}^{n+1/2} + h_{i+1}^{n+1/2}) + r_3(h_{i+1}^{n+1/2} + h_{i-1}^{n+1/2})^2 + C_i^{n+1}\Delta t/\sqrt{t}}{1 + r_2}. \tag{24}$$

Further stages must be performed alternately for the odd and the even nodes with (23) and (24), where n can have half-integer values as well.

At the final stage for the odd nodes, however, the time increment, and therefore the r quantities must be divided by two as follows

$$C_i^T = \frac{(1 - r_1/2)C_i^{T-1} + r_1/2(C_{i-1}^{T-1/2} + C_{i+1}^{T-1/2})}{1 + r_1/2}, \tag{25}$$

and, for Eq. (2)

$$h_i^T = \frac{(1 - r_2/2)h_i^{T-1} + r_2/2(h_{i-1}^{T-1/2} + h_{i+1}^{T-1/2}) + r_3/2(h_{i+1}^{T-1/2} + h_{i-1}^{T-1/2})^2 + C_i^T\Delta t/\sqrt{t}}{1 + r_2/2}. \tag{26}$$

The user must be aware that in each step, the latest available C and h values of the left and right neighbours are used. The properties of the LH method were exhaustively explained in our former studies,[17,18] and therefore, we skip them in this paper.

Numerical Experiment 1 Far from the cusps

We use the following parameters: $D = 3.5, \nu = 7, \lambda = 2, c_1 = 1, C_1 = 3$ and $C_2 = 0$. With these parameters, the argument of the tangent function is around π, so it is very far from half-integer π values and therefore no cusps can occur for any values of the space and time variable.

The initial condition is obtained simply by substituting the initial time into the analytical solution (10) and (13). Similarly, the appropriate Dirichlet boundary conditions are prescribed at the two ends of the interval using the analytical solutions (10) and (13). We produce the numerical solution at the interval $x \in [-25, 25]$, which is discretized by dividing it into 10000 equal parts, thus $\Delta x = 0.005$. The initial and the final time are $t^0 = 0.2$ and $t^{fin} = 2.2$. Then, the error as a function of the time step size Δt has been calculated for both examined methods and both functions. The results are displayed in Fig. 6. One can see that the LH is a stable second order method, while the standard FTCS is stable only below $\Delta t = 2\cdot 10^{-6}$. The residual errors (due to space discretization) are around 10^{-7} and $2\cdot 10^{-7}$ and for C and h, respectively. We present the graphs of the initial, final analytical and final numerical functions of C and h in Fig. 7, where the time step size for the LH method is $\Delta t = 2\cdot 10^{-3}$. We can conclude that in this case, the LH method can provide a qualitatively good solution with three orders of magnitude larger time step size than the explicit Euler discretization.

Experiment 2 Close to a cusp

We use the following parameters: $D = 0.5$, $\nu = 1$, $\lambda = 6$, $c_1 = 1$, $C_1 = 1$ and $C_2 = 0$. The space interval is $x \in [0, 1]$, the initial and the final time are $t^0 = 9$ and $t^{fin} = 9.6$. We will see that with these parameters, the cusp, which is travelling to the right, has just left the examined spatial region. We set $\Delta x = 0.0033$, thus we expect even smaller residual errors as in the previous experiment. The errors as a function of the time step size are displayed in Fig. 8. One can see that, unlike the FTCS scheme, the LH method is still stable. The residual error for C is indeed smaller than in Experiment 1, but the errors for h do not go down to these small values as expected but remain around $6.7\cdot 10^{-5}$ for both numerical algorithms. We present the graphs of the functions of C and h in Fig. 9, where the time step size for the LH method is $\Delta t = 4.7\cdot 10^{-3}$, which is again three orders of magnitude larger than the stability threshold for the FTCS method. However, the large residual error indicates that we are approaching the applicability limit of the methods, which is mostly due to the cusp and, to a smaller extent, the larger nonlinear coefficient.

Experiment 3 Focused on a cusp

We use the same parameters as in Experiment 2, except that now $\lambda = 3$, $x \in [0, 2]$, $t^0 = 1$, $t^{fin} = 1.1$, $\Delta x = 0.01$. We will see that with these parameters, the cusp is almost in the middle of the examined spatial region. The errors as a function of the time step size Δt are displayed in Fig. 10. One can see that the numerical methods for C are convergent as before, but the residual errors for h have large values for both numerical algorithms. The nature of this large error can be understood when one takes a look on the graphs of the functions in Fig. 11, where the smallest applied time step size $\Delta t = 3.8\cdot 10^{-7}$ was used for the LH method. The graphs in Fig. 11 show that according to the numerical solutions, the valley of the cusp is filled in instead of moving to the right. This phenomenon is the same for the FTCS

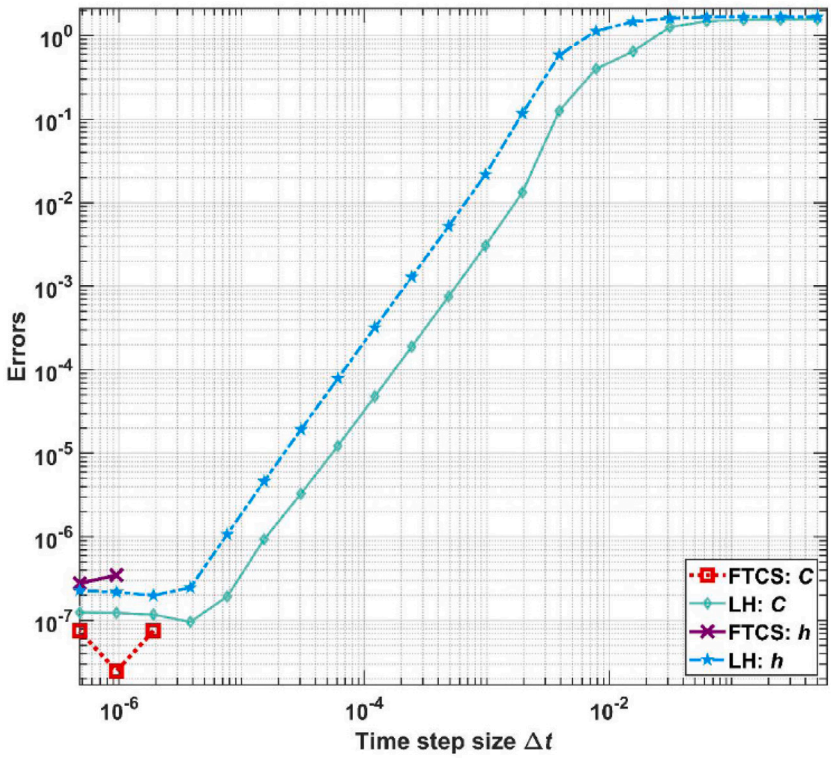

Fig. 6. Maximum errors as a function of time step size Δt for the numerical solutions of Eqs. (1)-(2) in case of the standard FTCS scheme, and the leapfrog-hopscotch method.

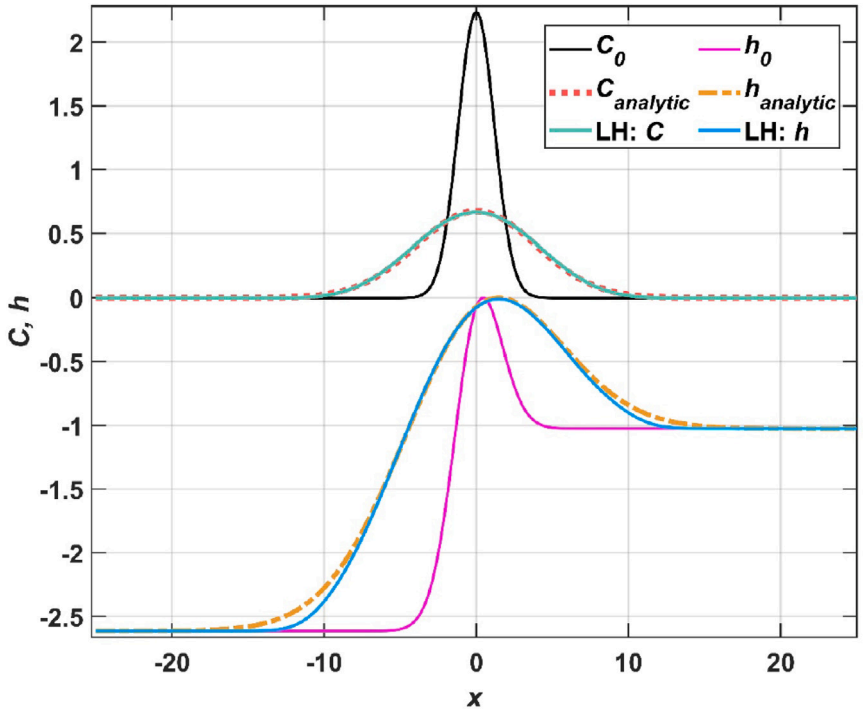

Fig. 7. Graphs of the C and h functions in Experiment 1. The time step size for the LH method is $\Delta t = 0.002$.

method as well, since the maximum difference between the FTCS and LH function values is $\Delta t = 6 \cdot 10^{-7}$. On the other hand, the LH is unstable for large time step sizes, albeit the stability threshold is still larger than for the FTCS scheme. For some other parameter values, *e.g.* for larger λ both algorithms are unstable for all examined time step sizes.

The reason for the failure of the finite difference numerical methods lies in the previously mentioned fact that the first derivative of the h function can be arbitrarily large. In fact, the first two terms on the right-hand side of (2) are increasing rapidly with opposite signs as we are getting closer to the cusp, but their sum increases much

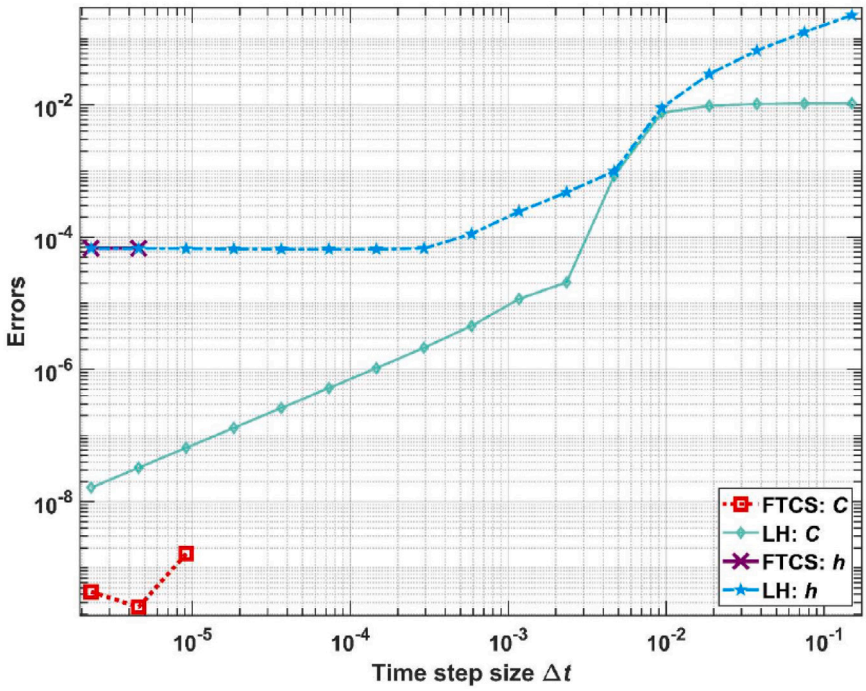

Fig. 8. Maximum errors as a function of time step size for the numerical solutions of Eqs. (1)-(2) in the case of the standard FTCS scheme, and the leapfrog-hopscotch method in Experiment 2.

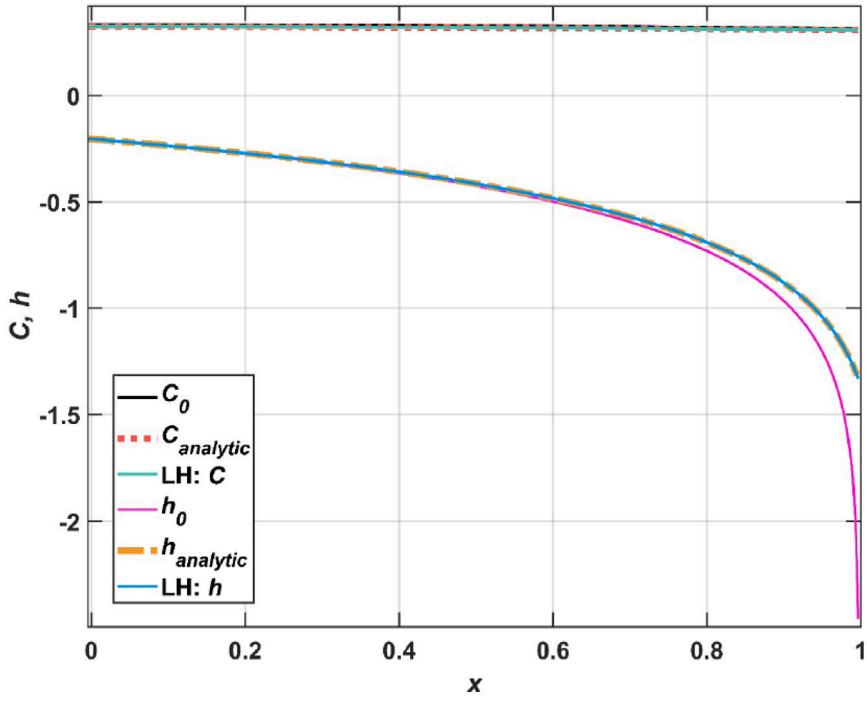

Fig. 9. Graphs of the C and h functions in Experiment 2. The time step size for the LH method is $\Delta t = 0.0047$.

slower. However, when the values of these derivatives are approximated numerically, the numerical error is proportional to the terms themselves and not to their sum, therefore the numerical error becomes comparable to the true values. The problem is that decreasing the space step size does not give a remedy but yields even more instability. On the other hand, decreasing the time step size cannot remove the inaccuracy coming from the error of the space discretization, so we can say that we reached the applicability limit of both the standard FTCS and the non-standard LH algorithms.

Experiment 4 Numerical reference solution

In order to study a case for which the condition for the analytical solution $4D = 2\nu$ is not valid, we set up a test problem with parameters and initial conditions far from those above. Let us fix the parameters of the equations to $D = 0.1$, $\nu = 1$, $\lambda = 14$. The space interval is $x \in [0, 1]$,

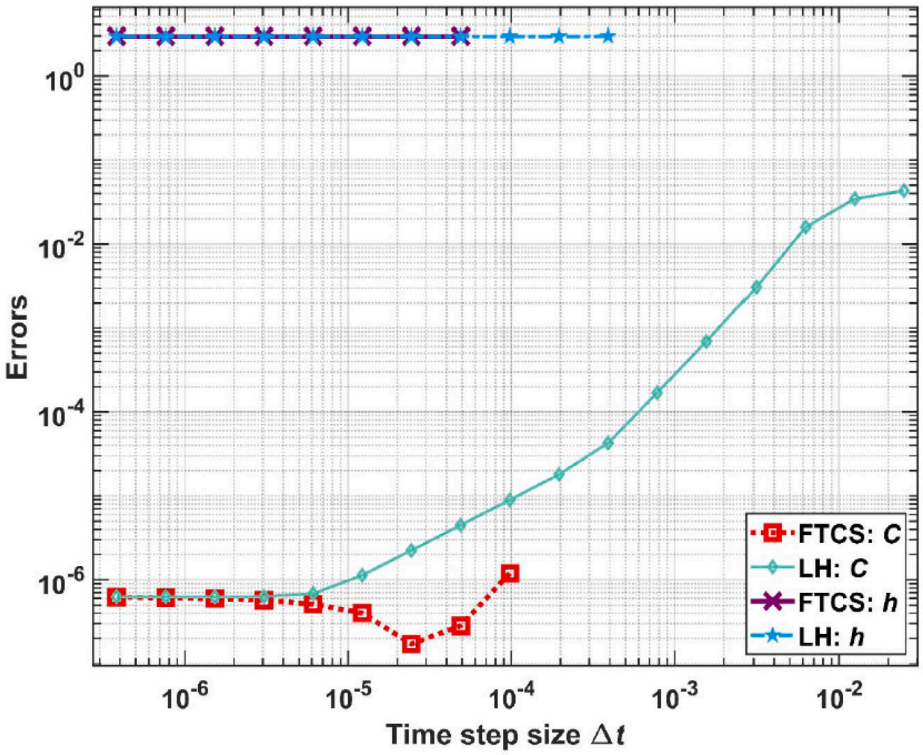

Fig. 10. Maximum errors as a function of time step size for the numerical solutions of Eqs. (1)-(2) in case of the standard FTCS scheme, and the LH method in Experiment 3.

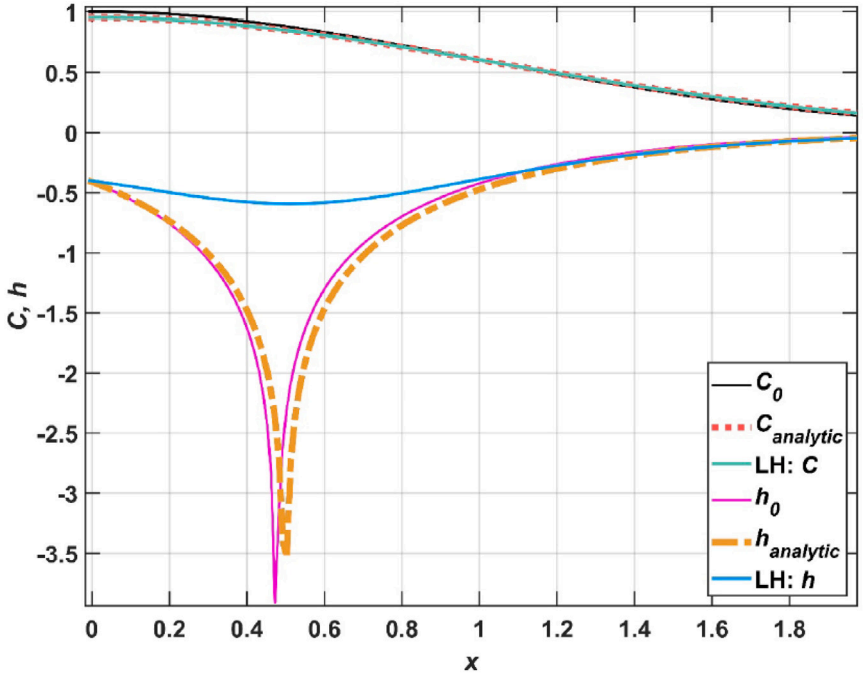

Fig. 11. Graphs of the C and h functions in Experiment 3.

the initial and the final time are $t^0 = 0.001$ and $t^{fin} = 0.0011$. The initial conditions are

$$C(x, t = 0) = 1.8 \cdot |sin(2\pi x)| - 1\,, \tag{27}$$

$$h(x, t = 0) = |sin(2\pi x)|\,, \tag{28}$$

and we set $\Delta x = 0.0025$ and periodic boundary conditions. We will see that with these parameters, there are valleys similar to cusps in both functions. Since the deep bottom of the valley of C has the same position as the bottom of the h valley, we expect that the interaction between the diffusion and the surface grow makes the valley of the surface deeper. The errors as a function of the time step size are displayed in Fig. 12. The solution provided by the FTCS scheme with the smallest time step size is used as the reference. One can see in the last Fig. 13, that the two numerical methods converge to the same solutions as in the previous three experiments. However, as the graphs

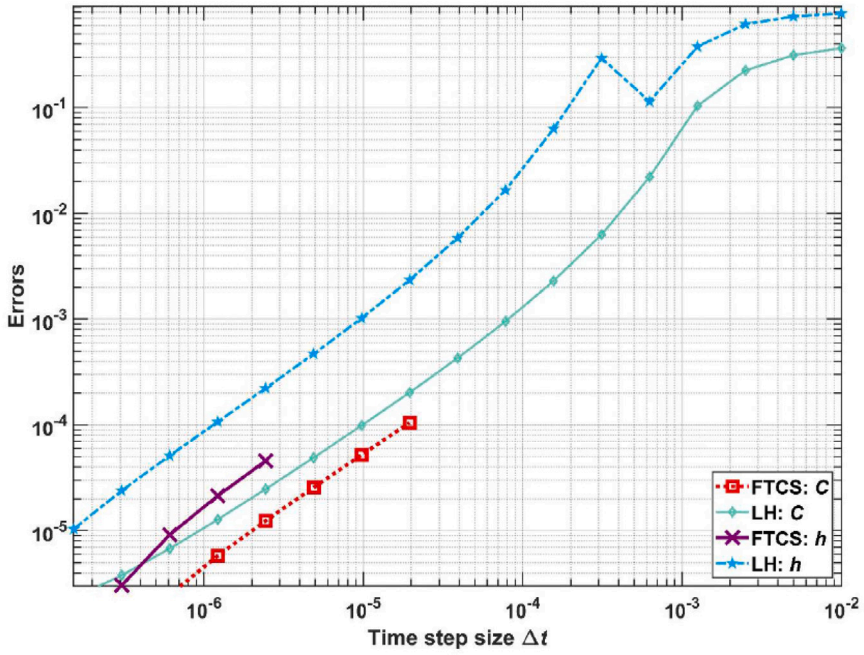

Fig. 12. Maximum errors as a function of time step size for the numerical solutions of Eqs. (1)-(2) in case of the standard FTCS scheme, and the LH method in Experiment 4.

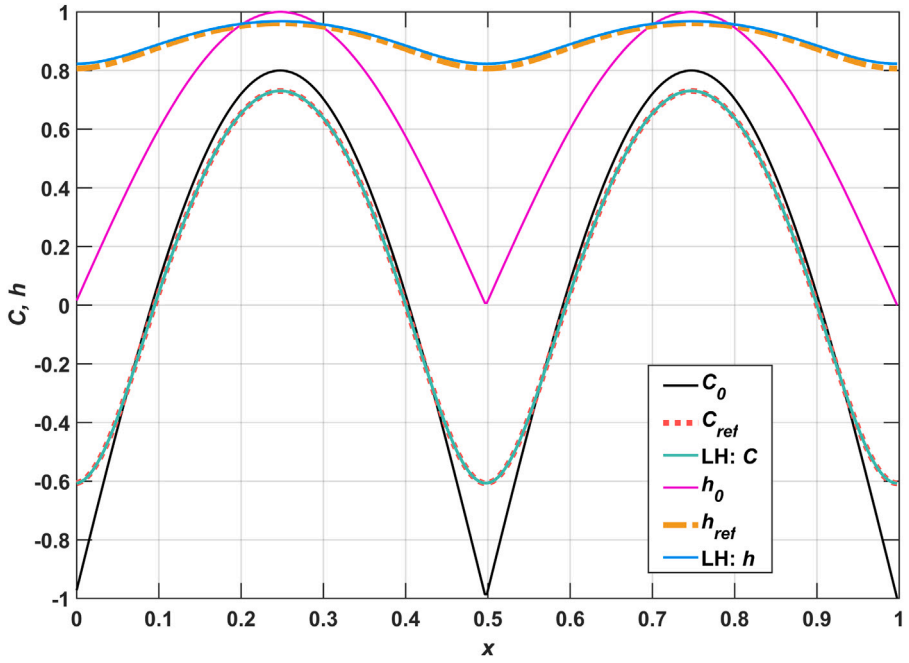

Fig. 13. Graphs of the C and h functions in Experiment 4. The time step size for the LH method is $\Delta t = 7.8 \cdot 10^{-5}$.

of the functions show, the valleys of both functions are significantly filled up, thus our expectations are not fulfilled. We note that whether this phenomenon is real or only the consequence of space discretization remains an open question.

4. Summary and outlook

In our study we presented and analysed a combined surface growth model in which a diffusion process served as a source term for the direct KPZ surface growing. The shape of the grown surface was given with a nontrivial analytic solution containing logarithmic, tangent and error functions. To make understanding of the solution possible, we presented a detailed parameter study and explained geometrically with a few neighbouring islands that formed and grew over time. In the second part of our study, we used the LH and the usual FTCS numerical schemes to investigate the model. We found that far from the cusps, the methods behave as expected: the FTCS was unstable above the CFL limit while stable and accurate below this. The LH was always stable, and acceptable solutions could be obtained with orders of larger time step size than the CFL limit. However, close to the cusps, both numerical methods failed to converge to the analytic solutions, even if the difference between them was very small. It is an interesting

question if there is any numerical scheme that exists which could solve this problem.

Further work is underway on how an analogue test can be performed by coupling a second-order wave equation to the KPZ equation. In a previous paper,[34] we have already investigated the KPZ equation with the travelling wave concept and found that analytical solutions can be derived for periodic noise. We think that this kind of analytical method can and will be applied to the current PDE system as well.

Declaration of competing interest

The authors have no relevant financial or non-financial interests to disclose.

Data availability

Data will be made available on request.

Acknowledgements

One of us (I.F. Barna) was supported by the NKFIH, the Hungarian National Research Development and Innovation Office. This study was supported by project no. 129257 implemented with the support provided from the National Research, Development and Innovation Fund of Hungary, financed under the K_18 funding scheme.

References

1. Barabási A-L. *Fractal Concepts in Surface Growth*. New York, NY, USA: Press Syndicate of the University of Cambridge; 1995.
2. Saito Y. *Statistical Physics of Crystal Growth*. Press: World Scientific; 1996.
3. Einax M, Dieterich W, Maass P. *Rev Modern Phys*. 2013;85:921.
4. Kardar M, Parisi G, Zhang Yi-C. *Phys Rev Lett*. 1986;56:889.
5. Sedov LI. *Similarity and Dimensional Methods in Mechanics*. CRC Press; 1993.
6. Barna IF, Bognár G, Hriczó K. *Math Model Anal*. 2016;21:83.
7. Barna IF. *Laser Phys*. 2014;24:086002.
8. Barna IF, Pocsai MA, Mátyás L. *J Gen Lie Theory Appl*. 2017;11:271.
9. Sarfraz M, Ahmed A, Khan M, Iqbal Ch MM, Azam M. *Waves Random Complex Media*. 2021:1–13.
10. Sarfraz M, Khan M. *Case Stud Therm Eng*. 2023;44:102857.
11. Sarfraz M, Khan M. *Numer Heat Transfer A: Appl*. 2024;85(3):351–363.
12. Barna IF, Bognár G, Guedda M, Hriczó K, Mátyás L. *Math Model Anal*. 2020;25:241.
13. Bognár G. *Appl Sci*. 2020;10:1422.
14. Sayfidinov O, Bognár G. *J Adv Appl Comput Math*. 2020;7:32.
15. Sayfidinov O, Bognár G. *Int J Appl Mech Eng*. 2021;26:206.
16. Mátyás L, Barna IF. *Romanian J Phys*. 2022;67:101.
17. Kovács E. *J Comput Appl Mech*. 2020;15:3–13.
18. Kovács E. *Numer Methods Partial Differ Equ*. 2020;37:2469.
19. Nagy Á, Issa O, Kareem H, Kovács E, Barna IF, Bognár G. *Computation*. 2021;9:92.
20. Mahmoud S, Kovács 1 E, Mátyás IFBarna L. *Mathematics*. 2022;10:2813.
21. Kovács E, Saleh M, Barna IF, Mátyás L. *Diffus Fund*. 2022;35:70.
22. Saleh M, Kovács E, Barna IF. *Algorithms*. 2023;16:184.
23. Khayrullaev H, Omle I, Kovács E. *Computation*. 2024;12:49.
24. Muravnik AB. *Complex Var Elliptic Equ*. 2019;64:736.
25. Arqub OA, Al-Smadi M. *J Porous Media*. 2020;23:783.
26. Arqub OA, Shawagfeh NT. *Jo Porous Media*. 2019;22:411.
27. Djennadi S, Shawagfeh N, Arqub OA. *Chaos Solitons Fractals*. 2021;150:111127.
28. Arqub OA, Tayebi S, Baleanu D, Osman MS, Mahmoud W, Alsulami H. *Results Phys*. 2022;41:105912.
29. Capietto A, Kloeden P, Mawhin J, Novo S, Ortega R. *Stability and Bifurcation Theory for Non-Autonomous Differential Equations*. Springer; 2013.
30. Carvalho AN, Langa JA, Robinson JC. *Attractors for Infinite-Dimensional Non-Autonomous Dynamical Systems*. Springer; 2013.
31. Cheban David N. *Global Attractors of Non-Autonomous Dissipative Dynamical Systems*. World Scientific Publishing; 2004.
32. D.W. Olver, Lozier FWJ, Boisvert RF, Clark CW. *NIST Handbook of Mathematical Functions*. Cambridge University Press; 2010.
33. Varró S, Földi P, Barna IF. *IOP Conf Series J Phys Conf Series*. 2019;1206:012005.
34. Barna IF, Bognár G, Mátyás L, Guedda M, Hriczó K. *Differential and Difference Equations with Applications*. 2019:239–255. In: Springer Proceedings in Mathematics & Statistics Series; vol. 333.